PCCP

Important Features of the Potential Energy Surface of the Methylamine Plus O(^{1}D) Reaction

Journal:	*Physical Chemistry Chemical Physics*
Manuscript ID	CP-ART-09-2019-005039.R1
Article Type:	Paper
Date Submitted by the Author:	17-Oct-2019
Complete List of Authors:	Wolf, Mark; University of Georgia , Center for Computational Quantum Chemsitry; Hoobler, Preston; Covenant College, Chemistry; University of Georgia Franklin College of Arts and Sciences, Center for Computational Quantum Chemistry Turney, Justin; University of Georgia, Center for Computational Chemistry Schaefer, Henry; University of Georgia, Computational Chemistry

Journal Name

ARTICLE TYPE

Cite this: DOI: 10.1039/xxxxxxxxxx

Important Features of the Potential Energy Surface of the Methylamine Plus O(^{1}D) Reaction †

Mark E. Wolf, Preston R. Hoobler, Justin M. Turney, and Henry F. Schaefer III*

Received Date
Accepted Date

DOI: 10.1039/xxxxxxxxxx

www.rsc.org/journalname

This research presents an *ab initio* characterization of the potential energy surface for the methylamine plus ^1D oxygen atom reaction, which may be relevant to interstellar chemistry. Geometries and harmonic vibrational frequencies were determined for all stationary points at the CCSD(T)/aug-cc-pVTZ level of theory. The focal point method along with several additive corrections was used to obtain reliable CCSDT(Q)/CBS potential energy surface features. Extensive conformational analysis and intrinsic reaction coordinate computations were performed to ensure accurate chemical connectivity of the stationary points. Five minima were determined to be possible products of this reaction and three novel transition states were found that were previously unreported or mislabeled in the literature. The pathways we present can be used to guide further searches for NH_2 containing species in the interstellar medium.

Introduction

Observation and characterization of interstellar molecules has been an expanding research field, as scientists have developed state-of-the-art methods to probe vast regions of space. A subset of this work has been identifying interstellar molecules that could lead to biological prerequisites, a primary target being amino acids.[1–5] In 1953, Miller proposed a means for the formation of prebiotic amino acids from primitive earth conditions.[6] Additional research has confirmed the existence of amino acids in meteorites, supporting the possibility that prebiotic molecules could form in the interstellar medium (ISM).[7,8] In fact, the Murchison meteorite which struck outside Murchison, Victoria, in Australia in 1969, was analyzed and found to contain 8 of the 20 biologically relevant amino acids.[9] Since then the search for other possible cosmic sources of prebiotic amino acids has exploded.[10,11] To date, the simplest amino acid glycine has been highly sought after, but has not been definitively confirmed in any interstellar region via spectroscopy.[12–17] There are numerous challenges in detecting amino acids in the ISM such as complex rotational bands and the fact that they are vulnerable to UV photodissociation.[18,19] These difficulties and the extreme conditions of space motivate understanding of the fundamental pathways that may form prerequisite molecules and guide the possible detection of amino acids.[20–24] Thus, the identification of smaller interstellar amines and has become an important task for astrochemists to fully understand the formation pathways of prebiotic molecules in space.[25–27]

The search for new types of chemical reactions in the ISM has been pushed forward by a synergy of experiment and theory. Gas phase ion-molecule chemistry has been understood historically as the dominant avenue for interstellar chemical reactions.[25,28] There are well documented examples where gas phase chemistry failed to properly predict the abundance of certain classes of molecules such as methanol[29], ethanol[30], and methyl formate within portions of the ISM.[28,31] One proposed solution was to consider radical-radical combinations on surfaces known as grains: particles of dust which form an icy surface on which radicals adhere.[22,32–36] Such gas-grain chemistry allows for the facile combination of radicals on these ice or dust surfaces and, eventually, diffusion into the gas phase. Moreover, molecules in the gas phase may also interact with these surfaces.[34] The gas-grain model was excellently described by Garodd and coworkers in 2008 where we direct the reader for more information.[35]

With the diversity of chemical processes available in the ISM, much information is needed to discern which reaction pathways are chemically relevant. Accurate potential energy surfaces are critical to determine if it is feasible for gas phase chemistry to produce relevant abundances of interstellar molecules, or if additional surface chemistry models are required. Regardless of the feasibility of the gas phase reactions in space, a detailed characterization of the potential energy surface can also aid in creating pure experimental samples of the desired products.[37]

Identification of interstellar amines has been an important scientific goal that has inspired spectroscopists for the last half century. One of the simplest amines, methylamine, has been observed in the star forming Sgr B2 and Ori A regions of

* *Center for Computational Quantum Chemistry, University of Georgia, 140 Cedar Street, Athens, Georgia 30602 United States of America. Fax: (706) 542-0406; Tel: (706) 542-2067; E-mail: ccq@uga.edu*

† Electronic Supplementary Information (ESI) available: [details of any supplementary information available should be included here]. See DOI: 10.1039/b000000x/

space.[38–40] Relatively few NH_2 containing compounds have been confidently identified in the ISM.[14,26,27,38,39,39,40] The gas-grain chemical model predicts the potential formation of more complex amines and related compounds such as: methoxyamine, N-methylhydroxylamine, and hydroxylamine, so there is good justification to keep looking.[35] These predictions and others have motivated recent searches for methoxyamine[27], methyl isocyanate[41], ethyl isocyanate[42], and hydroxylamine.[1,43] The success rate of future searches can potentially be increased by the aid of quantum chemical computations.

Many theoretical studies have examined the reaction pathways of molecules in the ISM leading to the formation of prebiotic molecules.[44–52] In 2013, Weaver and Hays proposed an alternate reaction pathway between methylamine and excited-state $O(^1D)$.[37] Methylamine has been predicted to be in high abundance in the gas phase by the previously mentioned gas-grain theoretical model as well as spectroscopically verified in star forming regions like Sgr B2. Similarly, the $O(^1D)$ atom has been shown to form via UV photolysis of many molecules with high abundances in the ISM making it a plausible candidate to react with methylamine.[53] The $O(^1D)$ atom has been shown experimentally to insert into both C-H and H-O bonds, unlike the ground state $O(^3P)$ atom.[54–56] Weaver and Hays proposed a potential energy surface where $O(^1D)$ reacts with methylamine to form N-methylhydroxylamine, methoxyamine, and aminomethanol via three reaction pathways. Their proposed potential energy surface, computed at the MP2/aug-cc-pVTZ level of theory, provides a simple route to form two amines that have only recently been spectroscopically verified in the ISM. The reaction studied by Weaver and Hays is analogous to previous studies by Balucani and coworkers, who examined the reaction pathways of other excited atoms reacting with small organic molecules.[57–59] The products of these reactions are prime molecules to study theoretically with the hope of understanding how they might form and provide guidance for detection of new amines in the ISM.[60] The potential energy surface proposed by Weaver and Hays predicts three major products of the $O(^1D)$ and methylamine combination: aminomethanol, N-methylhydroxylamine, and methoxyamine. Previous research has also examined species relevant to their potential energy surface. Goddard and coworkers have presented a viable mechanism to form aminomethanol from formaldehyde and ammonia and that it persists in the ISM with a decomposition rate less than 10^{-25} molecules s^{-1}.[61] Redondo and coworkers performed a theoretical study attempting to form glycine from protonated aminomethonal and formic acid but found the result nonviable.[46] Nevertheless, they demonstrated how an accurate theoretical potential energy surface was critical to understanding the chemistry in the ISM despite favorable a priori predictions of their negative result.[46]

Our work presents reliable features of the potential energy surface focusing on the products formed by the reaction of $O(^1D)$ and methylamine. The updated surface includes new transition states as well as corrected connectivities between stationary points. The transition states on that we characterize correspond to appropriate chemical processes and clarify the results of previous literature. Every structure presented in our work is an accurate geometry computed with state of the art methods in conjunction with extensive scans for all conformers. The relative energies presented are within chemical accuracy and trustworthy for further thermochemical applications. The results we present will be a useful step towards the identification of larger biological precursors in the ISM and will be helpful in determining the validity of gas-phase chemical pathways in the ISM for the formation of NH_2 containing species.

Methods

Initial reaction pathways found by scanning the reactivity of the $O(^1D)$ atom with methylamine using the software package ORCA[62] and the B3LYP functional[63] with Weigend-Ahlrichs def2-tzvp basis sets.[64] The same level of theory was used to scan for and optimize stationary point candidates, which, like the reactants, are all singlet species. These preliminary structures were then optimized using a restricted Hartree–Fock reference to find equilibrium geometries using coupled cluster theory with single, double, and perturbative triples excitations [CCSD(T)][65–68] with CFOUR2.0.[69] The Dunning augmented triple zeta basis set (aug-cc-pVTZ) was used for all geometry optimizations to capture possible long range interactions in the transition states.[70] Convergence criteria was set to 10^{-10} for the SCF density, coupled cluster amplitudes, and lambda equations. Harmonic vibrational frequencies were obtained at the CCSD(T)/aug-cc-pVTZ level of theory to confirm that the minima have no imaginary vibrational modes. We also demonstrate that transition states have exactly one imaginary normal mode, which corresponds to the appropriate chemical process. For transition states, intrinsic reaction coordinate computations were performed in Psi4[71] to verify connectivity between two adjacent minima.

To compare stationary points on the potential energy surface of the reaction shown in equation 1, we compute the reaction energy (ΔE) defined in equation 2.

$$O(^1D) + CH_3NH_2 \rightarrow \text{Product} \quad (1)$$

$$\Delta E = E_{\text{Products}} - E_{\text{Reactants}} \quad (2)$$

The $O(^1D)$ atom is well known to be a two determinant system and therefore cannot be well described with single reference coupled cluster methods. To account for this, we performed the focal point analysis of Allen and coworkers[72–75] on the $O(^3P)$ atom and methylamine and adjusted the result with the well established experimental singlet-triplet splitting of 45.37 kcal mol^{-1}[76] to more accurately compute the energy of the desired reactants: $O(^1D)$ and methylamine. The three point formula of Feller[77], equation 3, was used to extrapolate the HF/aug-cc-pVXZ (X = T, Q, 5) energies to the complete basis set limit (CBS). Likewise, the two point formula of Helgaker[78], equation 4, was used to extrapolate each post-Hartree–Fock incremental energy using the QZ and 5Z basis sets. To account for higher order electron correlation, additive corrections were included for full triples and perturbative quadruple excitiations.

$$E_{HF}(X) = E_{\mathrm{HF}}^{\infty} + ae^{-bX} \quad (3)$$

$$E_{corr}(X) = E_{\mathrm{corr}}^{\infty} + aX^{-3} \quad (4)$$

Preliminary computations on related systems have found that the CCSDT[79,80] correction was slightly basis set dependent and required augmented basis functions. The CCSDT additive correction was computed for the **TS1′** stationary point as a benchmark using the cc-pVTZ, jun-cc-pVTZ, jul-cc-pVTZ, and aug-cc-pVTZ basis sets.[81] CCSDT/aug-cc-pVTZ computations for all stationary points were computationally infeasible due to cost. To account for the basis set effects, we used a separate CCSDT/jul-cc-pVTZ correction (δE_{jul}). The CCSDT/jul-cc-pVTZ correction was affordable and within 0.05 kcal mol^{-1} of the CCSDT/aug-cc-pVTZ correction based on our benchmark. This correction is defined as the difference between the incremental difference of the CCSDT energy with an aug-cc-pVDZ basis and the incremental correction of the triples with jul-cc-pVTZ, as shown in equation 5. The CCSDT(Q)/aug-cc-pVDZ correction was included in the final focal point energies on each table.[82,83] This resulted in the CCSDT(Q)/CBS reaction energy ($\Delta \mathrm{E}_{\mathrm{CCSDT(Q)/CBS}}$).

$$\delta E_{\mathrm{jul}} = \delta(\mathrm{CCSDT/jul\text{-}cc\text{-}pVTZ}) - \delta(\mathrm{CCSDT/aug\text{-}cc\text{-}pVDZ}) \quad (5)$$

This energy was further improved upon by a series of standard additive corrections to account for other quantum effects shown in Equation 6.

$$\Delta H_{0\mathrm{K}} = \Delta E_{\mathrm{CCSDT(Q)/CBS}} + \delta E_{\mathrm{O(^1D)-O(^3P)}} + \delta E_{\mathrm{ZPVE}} + \delta E_{\mathrm{FC}} + \delta E_{\mathrm{jul}} + \delta E_{\mathrm{Rel}} + E_{\mathrm{DBOC}} \quad (6)$$

The zero point vibrational energy ($\delta \mathrm{E}_{\mathrm{ZPVE}}$) from the harmonic frequency computations was added to account for the ground state vibrational energy at 0 Kelvin ($\Delta H_{0\mathrm{K}}$). A frozen core correction was computed to account for the assumption that core electrons do not contribute to electron correlation. We define $\delta \mathrm{E}_{\mathrm{FC}}$ as the difference between the total energy of the system correlating all electrons minus the total energy of the same system with the core frozen at the CCSD(T)/aug-cc-pCVTZ level of theory. A scalar relativistic correction ($\delta \mathrm{E}_{\mathrm{rel}}$) was also added to compensate for the use of a non-relativistic Hamiltonian. The relativistic correction was computed using the DPT2[84] method at the CCSD(T)/aug-cc-pCVTZ level of theory. Finally, a diagonal Born–Oppenehimer correction, ($\delta \mathrm{E}_{\mathrm{DBOC}}$), was added to account for the clamped nuclei approximation and was computed at the Hartree–Fock level of theory with the aug-cc-pVTZ basis.[85,86] Our DBOC corrections also served as diagnostic to confirm that there were no non-adiabatic effects in our systems.

The stationary points were further analyzed using Natural Bond Orbital[87] (NBO) analysis as interfaced in ORCA[62] with NBO6.0.[88] NBO computations were performed with the standard aug-cc-pVDZ basis set and the B3LYP functional.

Results

Energetics

The CCSDT(Q)/CBS plus corrections characterization of the potential energy surface is presented in Figure 1. Table 1 contains the focal point analysis for each stationary point on the surface. All minima were converged to less than 0.47 kcal mol^{-1} for the CCSDT(Q) additive correction. The transition states exhibited much larger CCSDT(Q) corrections of about 1 kcal mol^{-1}, which can be seen in Table 2. To confirm the validity of this larger (Q) correction, we computed a full quadruples (CCSDTQ) correction[89–91] for **TS1'** with an aug-cc-pVDZ basis. We found a full-Q correction of 0.27 kcal mol^{-1} for **TS1'** indicating that we are well within chemical accuracy at the CCSDT(Q)/CBS level of theory. Therefore we expect that the uncertainty for all stationary points ,with respect to our level of theory, is no greater than than 0.27 kcal mol^{-1}. It is reasonable to assume that the other stationary points, being similar in nature, will also have small CCSDTQ corrections. Therefore we are confident that our computed relative energies are well within chemical accuracy.

Each additive correction behaved in a relatively uniform manner across the stationary points. The largest correction was the –45.37 kcal mol^{-1} addition to account for focal point extrapolation of the O(^{3}P) atom when O(^{1}D) is the reactant. Though this value is large, it is known with precision well beyond chemical accuracy and is not considered a source of computational error. The zero point vibrational correction ranged from 0.00_4 kcal mol^{-1} to 3.66 kcal mol^{-1} for all structures. The frozen core correction ranged from –0.01 kcal mol^{-1} to –0.71 kcal mol^{-1}. The CCSDT/jul-cc-pVTZ correction was very consistent and never exceeded 0.25 kcal mol^{-1}. Unsurprisingly, the relativistic correction was also small as our heaviest atom is oxygen. This value ranged from 0.00_3 kcal mol^{-1} to 0.20 kcal mol^{-1}. Finally, the DBOC was less than 0.10 kcal mol^{-1} for all of the stationary points, showing no evidence of non-adiabatic effects. The small and consistent magnitudes of the corrections for each stationary point are indicative of a trustworthy and accurate characteristics of the potential energy surface.

Minimum Geometries

Our computations found five equilibrium geometries characteristic of the potential energy surface. Each minimum was optimized and confirmed with a harmonic vibrational frequency computation at the CCSD(T)/aug-cc-pVTZ level of theory. Tables containing the harmonic frequencies can be found in the Supporting Information. Each structure was analyzed for other possible conformers. The lowest energy conformer of each structure is presented in Figure 1. Cartesian coordinates are available for all optimized geometries, including higher energy conformers, in the Supporting Information. The following section is a detailed description of each minimum characteristic of the methylamine and O(^1D) potential energy surface, ordered from lowest to highest $\Delta H_{0\mathrm{K}}$ and comparisons to the MP2/aug-cc-pVTZ geometries

Table 1 Incremental focal point table for the five minimum structure on the potential energy surface relative to the reactants in kcal mol^{-1}. Bracketed terms are either extrapolated values or additive corrections. The CCSDT(Q)/CBS estimates were further improved by a series of additive corrections: $\delta E_{O(^1D)-O(^3P)} + \delta E_{ZPVE} + \delta E_{FC} + \delta E_{jul} + \delta E_{Rel} + E_{DBOC}$.

M1: aminomethanol							
	HF	+δ MP2	+δ CCSD	+δ (T)	+δ T	+δ (Q)	NET
aug–cc–pVDZ	–54.73	–49.83	+11.53	–2.98	+0.15	–0.34	[–96.20]
aug–cc–pVTZ	–55.58	–54.14	+12.36	–4.06	[+0.15]	[–0.34]	[–101.61]
aug–cc–pVQZ	–55.77	–56.19	+12.49	–4.27	[+0.15]	[–0.34]	[–103.94]
aug–cc–pV5Z	–55.74	–56.88	+12.63	–4.34	[+0.15]	[–0.34]	[–104.52]
CBS LIMIT	[–55.70]	[–57.61]	[+12.79]	[–4.42]	[+0.15]	[–0.34]	[–105.13]
$E_{CCSDT(Q)/CBS+\Delta}$ = –105.13–45.37+3.54–0.71+0.17+0.20–0.06 = **–147.36**							
M2: methylamine oxide							
	HF	+δ MP2	+δ CCSD	+δ (T)	+δ T	+δ (Q)	NET
aug–cc–pVDZ	+4.07	–50.65	+10.05	–3.65	+0.13	–0.46	[–40.50]
aug–cc–pVTZ	+3.89	–55.00	+11.13	–4.86	[+0.13]	[–0.46]	[–45.17]
aug–cc–pVQZ	+3.82	–56.85	+11.34	–5.10	[+0.13]	[–0.46]	[–47.11]
aug–cc–pV5Z	+3.87	–57.48	+11.50	–5.18	[+0.13]	[–0.46]	[–47.62]
CBS LIMIT	[+3.91]	[–58.15]	[+11.67]	[–5.27]	[+0.13]	[–0.46]	[–48.16]
$E_{CCSDT(Q)/CBS+\Delta}$ = –48.16–45.37+3.66–0.59+0.19+0.13-0.03 = **–90.17**							
M3: N-methylhydroxylamine							
	HF	+δ MP2	+δ CCSD	+δ (T)	+δ T	+δ (Q)	NET
aug–cc–pVDZ	–15.75	–50.81	+9.75	–3.45	+0.13	–0.47	[–60.61]
aug–cc–pVTZ	–16.26	–55.09	+10.87	–4.62	[+0.13]	[–0.47]	[–65.43]
aug–cc–pVQZ	–16.38	–56.87	+11.11	–4.85	[+0.13]	[–0.47]	[–67.33]
aug–cc–pV5Z	–16.34	–57.48	+11.27	–4.93	[+0.13]	[–0.47]	[–67.82]
CBS LIMIT	[–16.30]	[–58.12]	[+11.44]	[–5.02]	[+0.13]	[–0.47]	[–68.34]
$E_{CCSDT(Q)/CBS+\Delta}$ =–68.34–45.37+2.84–0.59+0.19+0.13–0.03 = **–111.17**							
M4: CH_3OHNH							
	HF	+δ MP2	+δ CCSD	+δ (T)	+δ T	+δ (Q)	NET
aug–cc–pVDZ	+47.12	–45.42	+6.40	–4.20	–0.04	–0.46	[+3.39]
aug–cc–pVTZ	+46.17	–49.09	+7.55	–5.21	[–0.04]	[–0.46]	[–1.09]
aug–cc–pVQZ	+46.27	–50.51	+7.88	–5.43	[–0.04]	[–0.46]	[–2.30]
aug–cc–pV5Z	+46.32	–51.05	+8.09	–5.50	[–0.04]	[–0.46]	[–2.65]
CBS LIMIT	[+46.35]	[–51.62]	[+8.31]	[–5.58]	[–0.04]	[–0.46]	[–3.05]
$E_{CCSDT(Q)/CBS+\Delta}$ = –3.05–45.37+1.50–0.27+0.15+0.05-0.02 = **–47.01**							
M5: methoxyamine							
	HF	+δ MP2	+δ CCSD	+δ (T)	+δ T	+δ (Q)	NET
aug–cc–pVDZ	–10.64	–49.63	+9.19	–3.46	+0.12	–0.46	[–54.88]
aug–cc–pVTZ	–12.03	–53.61	+10.33	–4.57	[+0.12]	[–0.46]	[–60.21]
aug–cc–pVQZ	–12.04	–55.29	+10.56	–4.80	[+0.12]	[–0.46]	[–61.91]
aug–cc–pV5Z	–12.02	–55.90	+10.71	–4.88	[+0.12]	[–0.46]	[–62.42]
CBS LIMIT	[-11.99]	[–56.53]	[+10.87]	[–4.97]	[+0.12]	[–0.46]	[–62.96]
$E_{CCSDT(Q)/CBS+\Delta}$ =–62.96–45.37+2.64–0.52+0.18+0.13–.01 = **–105.91**							

Table 2 Incremental focal point table for the four transition state structures on the potential energy surface relative to the reactants in kcal mol^{-1}. Bracketed terms are either extrapolated values or additive corrections. The CCSDT(Q)/CBS estimates were further improved by a series of additive corrections: $\delta E_{O(^1D)-O(^3P)} + \delta E_{ZPVE} + \delta E_{FC} + \delta E_{jul} + \delta E_{Rel} + E_{DBOC}$.

TS1							
	HF	+δ MP2	+δ CCSD	+δ (T)	+δ T	+δ (Q)	NET
aug–cc–pVDZ	+43.31	–62.15	+12.45	–5.68	+0.21	–0.90	[–12.77]
aug–cc–pVTZ	+42.83	–66.53	+13.81	–7.13	[+0.21]	[–0.90]	[–17.70]
aug–cc–pVQZ	+42.97	–68.37	+14.16	–7.42	[+0.21]	[–0.90]	[–19.34]
aug–cc–pV5Z	+43.05	–68.98	+14.38	–7.52	[+0.21]	[–0.90]	[–19.76]
CBS LIMIT	[+43.09]	[–69.62]	[+14.60]	[–7.62]	[+0.21]	[–0.90]	[–20.24]
$E_{CCSDT(Q)/CBS+\Delta}$ = –20.24–45.37+0.00$_4$–0.55+0.22+0.06–0.05 = **–65.93**							
TS1'							
	HF	+δ MP2	+δ CCSD	+δ (T)	+δ T	+δ (Q)	NET
aug–cc–pVDZ	+82.14	–62.79	+11.50	–6.92	–0.02	–0.99	[+22.91]
aug–cc–pVTZ	+81.67	–66.90	+13.14	–8.35	[–0.02]	[–0.99]	[+18.56]
aug–cc–pVQZ	+81.92	–68.62	+13.58	–8.63	[–0.02]	[–0.99]	[+17.23]
aug–cc–pV5Z	+81.99	–69.22	+13.82	–8.73	[–0.02]	[–0.99]	[+16.85]
CBS LIMIT	[+82.02]	[–69.84]	[+14.08]	[–8.84]	[–0.02]	[–0.99]	[+16.41]
$E_{CCSDT(Q)/CBS+\Delta}$ =+16.41–45.37+0.71–0.59+0.23+0.13+0.04 = **–28.45**							
TS2							
	HF	+δ MP2	+δ CCSD	+δ (T)	+δ T	+δ (Q)	NET
aug–cc–pVDZ	+98.78	–60.49	+9.03	–7.95	–0.28	–1.16	[+37.92]
aug–cc–pVTZ	+98.70	–64.24	+10.81	–9.28	[–0.28]	[–1.16]	[+34.55]
aug–cc–pVQZ	+99.01	–65.69	+11.33	–9.24	[–0.28]	[–1.16]	[+33.66]
aug–cc–pV5Z	+99.09	–66.20	+11.61	–9.64	[–0.28]	[–1.16]	[+33.41]
CBS LIMIT	[+99.12]	[–66.74]	[+11.91]	[–9.74]	[–0.28]	[–1.16]	[+33.09]
$E_{CCSDT(Q)/CBS+\Delta}$ =+33.09–45.37–0.31 –0.01+0.20–0.01+0.03 = **–12.38**							
TS3							
	HF	+δ MP2	+δ CCSD	+δ (T)	+δ T	+δ (Q)	NET
aug–cc–pVDZ	+59.88	–52.32	+7.23	–5.89	–0.07	–0.76	[+8.08]
aug–cc–pVTZ	+58.95	–56.09	+8.64	–7.07	[–0.07]	[–0.76]	[+3.60]
aug–cc–pVQZ	+59.15	–57.49	+9.05	–7.31	[–0.07]	[–0.76]	[+2.57]
aug–cc–pV5Z	+59.22	–58.01	+9.28	–7.40	[–0.07]	[–0.76]	[+2.27]
CBS LIMIT	[+59.25]	[–58.55]	[+9.53]	[–7.49]	[–0.07]	[–0.76]	[+1.91]
$E_{CCSDT(Q)/CBS+\Delta}$ =+1.91–45.37–0.80–0.23+0.18+0.00$_3$–0.02 = **–44.33**							

given by Weaver and coworkers.[37] For most of the geometries, the less reliable MP2 results predicts shorter bond lengths than our CCSD(T) values.

Structure **M1**, aminomethanol, is the the lowest minimum on the potential energy surface with a ΔH_{0K} value of –147.36 kcal mol^{-1}. The lowest conformer (Conformer 1), shown in Figure 2, is a C_1 structure with the hydroxyl hydrogen rotated out of plane with respect to the O-C-N backbone and the amine group *trans* to the two closest methyl hydrogens. The O-C and C-N bond lengths are 1.431 and 1.422 Å, respectively. The C-N bond is shortened compared to the 1.470 Å in methylamine. The O-C bond length has almost exact agreement with the MP2/aug-cc-pVTZ results of Weaver and Hays, but our computed C-N bond is 0.014 Å shorter.[37] Aminomethanol has three additional conformers. Conformer 2 is a C_s structure, where the hydroxyl hydrogen is rotated back into the plane of the molecule resulting in a 0.22 kcal mol^{-1} increase in energy relative to Conformer 1. Conformer 3 is 0.73 kcal mol^{-1} higher than Conformer 1 and is characterized by a twist in the amino group out of plane, as well as a rotation of the hydroxyl group aligned with the nitrogen atom. Conformer 4 is significantly higher in energy at 4.04 kcal mol^{-1} than Conformer 1 and is similar to the C_s conformer but with the amino group rotated out of plane to break the C_s symmetry.

The next structure that lies closest in energy to **M1** is **M3** or N-methylhydroxylamine (Figure 3) at –111.17 kcal mol^{-1}. **M3** has 1.451 and 1.463 Å for the O-N and C-N distances, respectively. This means that substitution of an amino hydrogen in methy-

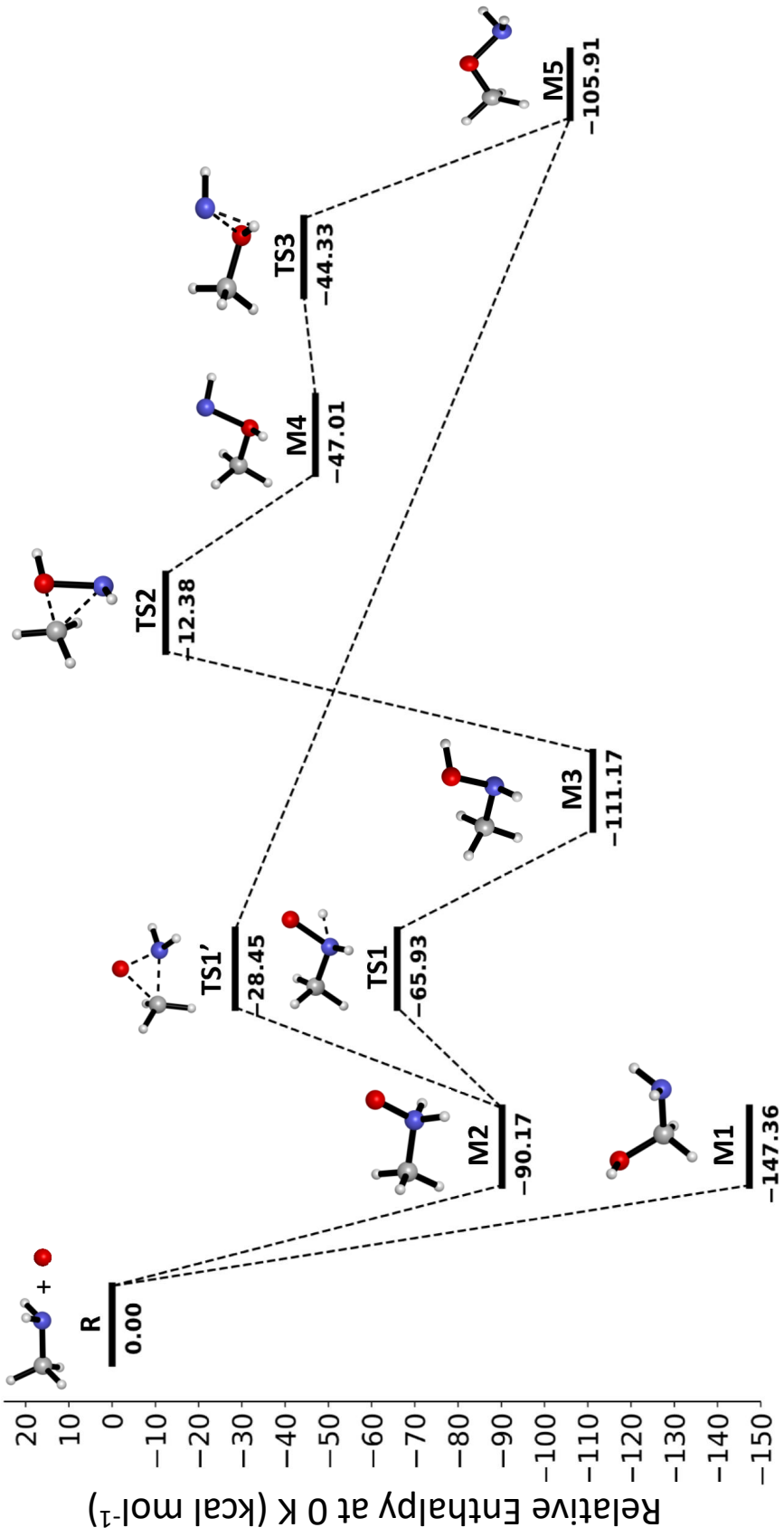

Fig. 1 The CCSDT(Q)/CBS +Δ stationary points associated with the reaction between methylamine and the excited-state $O(^1D)$ atom. Relative zero Kelvin enthalpies are shown in kcal mol^{-1}. Five minimum equilibrium geometries exist on our surface and are discussed in depth in the results section.

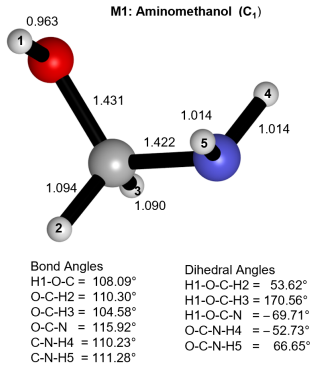

Fig. 2 The CCSD(T)/aug-cc-pVTZ optimized equilibrium geometry of aminomethanol (**M1**). The bond lengths are shown in Angstroms with relevant bond angles and dihederal angles shown below.

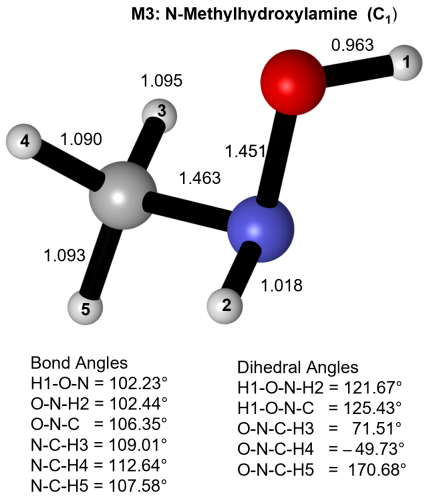

Fig. 3 The CCSD(T)/aug-cc-pVTZ optimized equilibrium geometry of n-methylhydroxylamine (**M3**). The bond lengths are shown in Angstroms with relevant bond angles and dihederal angles shown below.

lamine with a hydroxy group slightly shortens the C-N bond by 0.007 Å. The MP2 results of Weaver and Hays predicted somewhat shorter O-N and C-N bonds of 1.446 and 1.456 Å, respectively. We found two minimum conformers by scanning over the methyl and hydroxyl rotations. Conformer 1 has a –125.43 degree dihederal angle between the hydroxyl hydrogen and the O-N-C backbone. Rotation of this angle to 60 degrees results in Conformer 2, that is 3.44 kcal mol^{-1} higher in energy. In Conformer 2 the energy is raised because the hydroxyl hydrogen is in an unfavorable proximity to the amino hydrogen.

M5 (Figure 4) is slightly higher in energy than **M3** with a ΔH_{0K} of –105.91 kcal mol^{-1} and is classified as methoxyamine. The C-O bond in **M5** is the smallest of all the minimum structures with a length of 1.422 Å which is still larger than the 1.417 Å bond predicted by Weaver and Hays[37]. The C-O bond is slightly longer at 1.444 Å, which is significantly larger than the MP2 bond length of 1.417 Å. **M5** has two conformers relating to the *cis* or *trans* orientation of the amino group with respect to the methyl group. Conformer 1, the *trans* structure, is predicted to lie 2.29 kcal mol^{-1} lower in energy than Conformer 2. The unfavorable interactions between the amino and methyl hydrogens account for the *cis* conformation having a higher ΔH_{0K}. Both conformers maintain C_s symmetry.

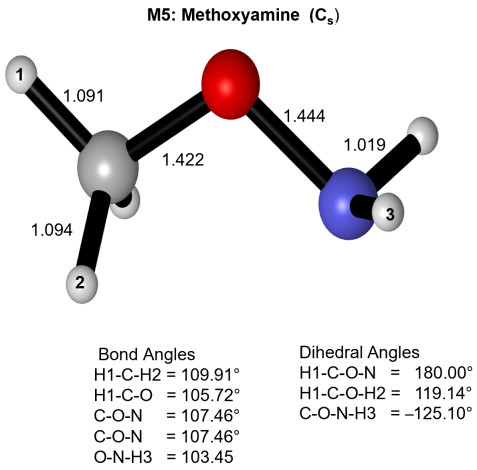

Fig. 4 The CCSD(T)/aug-cc-pVTZ optimized equilibrium geometry of methoxyamine (**M5**). The bond lengths are shown in Angstroms with relevant bond angles and dihederal angles shown below.

Perhaps the most interesting minimum is **M2** or methylamine oxide (Figure 5). This molecule has C_s symmetry and a staggered geometry with respect to the methyl group and the NH_2O group about the C-N bond. The ΔH_{0K} of **M2** is –90.17 kcal mol^{-1}. The most defining feature of this molecule is the tetravalent nitrogen which is bonded to a carbon, two hydrogens, and an oxygen. The oxygen has only a single bond and therefore a formal charge of -1, which balances with the formal charge of $+1$ on the tetravalent nitrogen. Unlike many of the previous structures, the C-N bond of **M2** (1.486 Å) is significantly longer than the C-N bond in methylamine by 0.016 Å and longer than the C-N bond for any other minima. The O-N bond in **M2** is the shortest of all O-N bonds presented in this work at 1.371 Å. Weaver and coworkers

again predicted shorter C-N and O-N bonds of 1.483 and 1.355 Å, respectively.

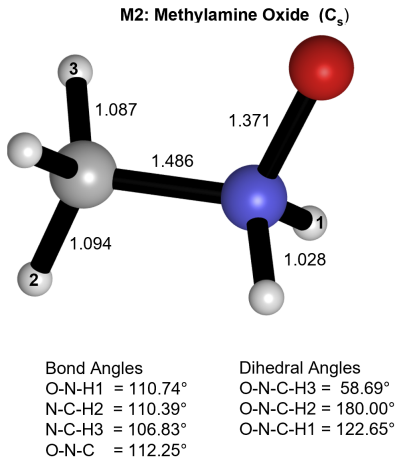

Fig. 5 The CCSD(T)/aug-cc-pVTZ optimized equilibrium geometry of methylamine oxide (**M2**). The bond lengths are shown in Angstroms with relevant bond angles and dihederal angles shown below.

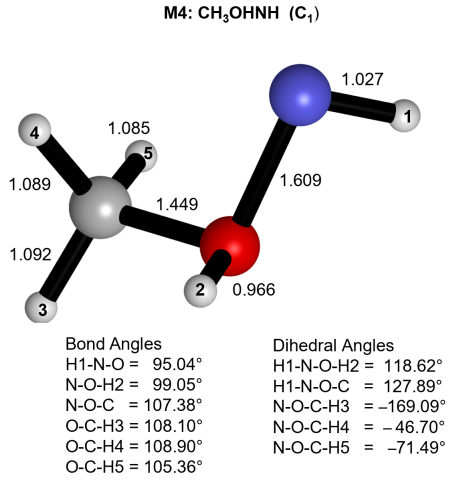

Fig. 6 The CCSD(T)/aug-cc-pVTZ optimized equilibrium geometry of CH_3OHNH (**M4**). The bond lengths are shown in Angstroms with relevant bond angles and dihederal angles shown below.

The final equilibrium geometry **M4** (CH_3OHNH) is the highest energy minimum that we found (see Figure 6). This structure has C_1 symmetry and a ΔH_{0K} of –47.01 kcal mol^{-1}. The geometry of **M4** resembles that of **M3** but with the oxygen and nitrogen positions swapped. This unusual structure also has nonzero formal charges with a -1 and $+1$ formal charge for nitrogen and oxygen respectively. The C-O bond in **M4** is 0.014 Å shorter than the geometrically analogous C-N bond in **M3**. However, the most substantial change from **M3** is the 0.158 Å elongation of the O-N bond in **M4**. A second higher energy conformer was found by rotating the H-N-O-C dihderal angle from –127.89 degrees to –57.15 degrees which places the amino hydrogen in unfavorable proximity to the methyl group. Conformer 2 is 3.69 kcal mol^{-1} higher in energy than Conformer 1 on the potential energy surface.

Reaction Pathways

The characteristics of the potential energy surface presented in this research contain novel and corrected pathways for the reaction of methylamine and the O(^{1}D) atom. Extensive DFT scans of the O(^{1}D) atom reacting with methylamine determined that there are two possible barrierless processes that the initial reactants can undergo. There was no indication of the formation of a pre-reactive complex in either process. The first is an insertion of the oxygen atom into a C-H bond on methylamine to form **M1**. **M1** is the lowest energy product on the surface (–147.36 kcal mol^{-1}) and we would therefore expect **M1** to be the dominant product. Further scans showed no evidence that **M1** could continue on a reaction pathway to form any other minima.

The second initial pathway leads to a more varied chemistry of greater interest within this study. The alternative to the formation of **M1** is the barrierless addition of the O(^{1}D) atom to the nitrogen of methylamine to form **M2**. Even though **M1** is significantly lower in energy than **M2**, the fact that **M2** is 90.17 kcal mol^{-1} lower in energy than the reactants and also has no barrier makes it a quite viable pathway. If **M2** is formed, it is more likely to proceed along the surface than dissociate back into the initial reactants because energetic barriers to further reactions are much lower than dissociating back into the reactants. From **M2**, there are two possible routes for the reaction to proceed: 1) a hydrogen migration from the nitrogen to the oxygen (**TS1**). 2) The insertion of the oxygen into the nitrogen and carbon bond through an "epoxy-like" transition state (**TS1′**). Complete focal point analyses for all transition states are found in Table 2.

The first option has the lowest energy barrier of 24.24 kcal mol^{-1} and proceeds through **TS1**, Figure 7, to form **M3**. This connectivity was confirmed through an IRC computation. The geometry of **TS1** is quite similar to **M2** except for an opening of the C-N-H5 angle from 110.74 degrees to 125.45 degrees as the oxygen starts to interact with an amino hydrogen, also breaking C_s symmetry. The geometry presented was confirmed to be a transition state with a single large imaginary harmonic vibrational frequency of 1659i cm^{-1}, corresponding to the oxygen abstracting a hydrogen from the nitrogen. NBO was used to obtain the natural bond order between key atoms in the reaction to further confirm our intuition. In the reactant **M2**, the NBO indicates three lone pairs on the oxygen atom and no formation of an O-H bond. The product, **M3**, has only one lone pair on oxygen and an O-H bond order of 1.00 as we expect for a single bond. The transition state shows 2.95 lone pair occupation on the oxygen atom and a O-H bond order that is still negligible, indicating that it is very much reactant like. This agrees with the chemical intuition of Hammond's postulate for an exothermic reaction[92].

The second pathway from **M2** is the formation of an "epoxy-like" **TS1′** (Figure 9) where the oxygen swings between the C-N bond and starts to insert between them to eventually form **M5**. The barrier accompanying this transition state is large at 61.72 kcal mol^{-1} but is still energetically submerged by 28.45 kcal mol^{-1} with respect to the reactants. The oxygen in-

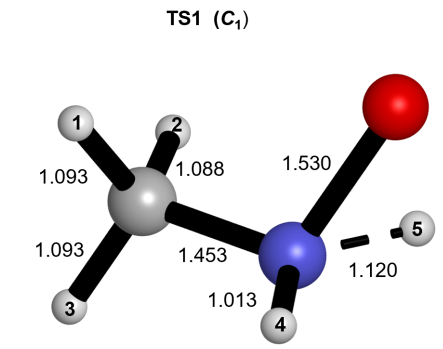

Fig. 7 The CCSD(T)/aug-cc-pVTZ optimized transition state geometry of **TS1**, connecting **M2** and **M3** . The bond lengths are shown in angstroms with relevant bond angles and dihederal angles shown below.

sertion stretches the C-N bond to 1.749 Å, as well as forming an elongated O-C bond of 1.873 Å and a O-N bond of 1.478 Å. **TS1′** has an single imaginary vibrational frequency of 1115i cm^{-1}. The NBO computations confirm that **TS1′** is also more similar to **M2** than **M5**. The transition state oxygen possesses an average of 2.55 electrons compared to 1.97 in methoxyamine. Likewise, the O-C bond orders are 0.00 , 0.43, and 1.03 for the reactant, transition state, and product, respectively. **TS1′** has more of a mixture of **M2** and **M5** than **TS1** but still manages to satisfy Hammond's postulate for an exothermic reaction.

M5 is considered a terminal product on our surface and does not react to form any other new molecules. **M3**, however, has the possibility of further reacting. **M3** has one possible forward pathway where the hydroxyl group swings down and the oxygen inserts into the C-N bond to form **TS2** and eventually lead to **M4**. **TS2** is quite similar to **TS1′** in that each forms a three-membered ring between the oxygen, nitrogen, and carbon atoms. This process can also be described as a methyl shift between the oxygen and nitrogen. The barrier for a reaction proceeding from **M3** through **TS2** is a massive 98.79 kcal mol^{-1}. Despite the higher barrier, **TS2** is 12.38 kcal mol^{-1} lower in energy than the reactants and is still a plausible pathway, the barrier for **M3** to react backwards through **TS1** is only 45.24 kcal mol^{-1}. Therefore it is more probable for **M3** to react backwards to **M2** rather than to **M4**. NBO computations give C-O bond orders of 0.00, 0.54, and 1.03 and oxygen lone pair values of 2.00, 1.46, and 0.99 for **M3** , **TS2**, and **M4**, respectively. In this case Hammond's postulate is supported for an endothermic reaction as the transition state is slightly more similar to the product.

M4 is an unlikely minimum that is 47.01 kcal mol^{-1} lower in energy than the reactants. Once **M4** is formed, there is an energy barrier of only 2.68 kcal mol^{-1} to proceed through **TS3** which leads to the final product **M5**. This will be the dominant path compared to the backward reaction to **M3** which involves a barrier of 34.63 kcal mol^{-1}. **TS3** has a single imaginary vibrational mode of 1054i cm^{-1} which corresponds to the chemical process of the hydrogen transferring from the oxygen to the nitrogen, as shown in Figure 11. The most notable feature is the long O-N bond that is stretched to 1.697 Å. Again, the natural bond order analysis confirms that the transition state is more like the reactant rather than the final product methoxyamine. The nitrogen lone pair occupancy is 2.00 for CH_3OHNH and 1.95 for **TS2**. Methoxyamine has a nitrogen lone pair occupancy of 1.00 since the nitrogen has only one lone pair when bonded to two hydrogens and oxygen. For all four of the major transition states, Hammond's postulate agrees with our NBO computations, thus agreeing with our chemical intuition.

Discussion

Characterization of our potential energy surface predicts five minimum structures which might all be expected to contribute to rotational spectra. Our research provides two important corrections to the current potential energy surfaces in the literature. The primary correction is the incorrect assignment of the transition state, **TS1′** that links **M2** and **M5**.[37] Our research has reassigned their transition state geometry as similar to our **M4** structure. The stationary points we present elucidate the correct chemical connectivity of **M4**. This reassignment allowed us to optimize a new transition state to directly connect **M2** and **M5** and confirm this by IRC computations. This increases the overall energetic barrier for this process from 50.0 kcal mol^{-1} predicted by Weaver and Hays to our estimate of 61.7 kcal mol^{-1}. This is important because the pathway through **TS1′** is the lowest energy pathway for the formation of **M5**, so an accurate transition state and barrier height are necessary to predict its abundance.

The second major correction is that we were able to optimize an additional transition state (**TS2**) that links **M3** and **M4**. **TS2** has a major barrier of 98.8 kcal mol^{-1} with respect to **M3**, so it is unlikely that this will be a dominant reaction pathway. Nevertheless, it is energetically submerged with respect to reactants and is a possibility given the free energy released by the reactants. This pathway also properly contextualizes **M4** as a proper minimum which is 64.2 kcal mol^{-1} higher in energy than **M3**. The reaction barrier for **M4** to proceed to **M5** is a minimal 2.7 kcal mol^{-1}. Therefore we have two possible pathways to reach **M5**, both of which we present with novel transition states that are previously unreported in the literature.

Both methylamine and O(^1D)[38,53] have been confirmed in the ISM and barrierless entrance channels make the chemistry we present plausible for the low temperature conditions of space. Therefore, it is of interest to comment on which products we predict to persist from this reaction. Figure 8 depicts the potential energy surface with **M1** set to zero to more easily visualize reaction barriers for each minimum. It seems obvious that **M1** will be the dominant product as its formation has no barrier and it is the lowest potential well on our surface. We can now make accurate predictions for the other minima which are not as obvious. **M2** is also an initial product and sits in an energy well of at least 24.8 kcal mol^{-1} below the reactants, so it is expected to persist with relatively high abundance. To the best of our

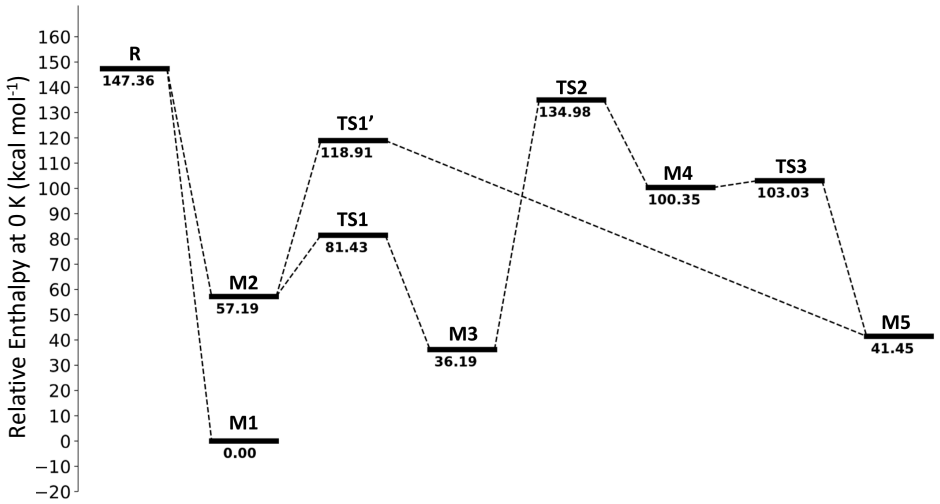

Fig. 8 The CCSDT(Q)/CBS +Δ stationary points associated with the reaction between methylamine and the excited-state O(^{1}D) atom. Relative zero Kelvin enthalpies are shown in kcal mol^{-1} with **M1** as the reference.

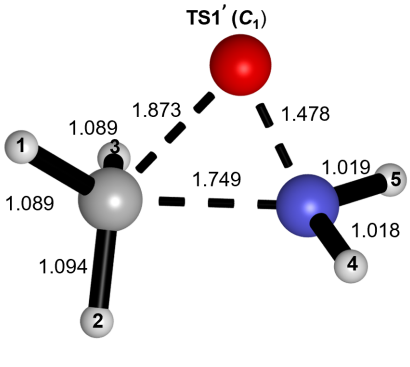

Bond Angles
H1-C-H3 = 112.35°
H1-C-H2 = 109.93°
H1-C-N = 128.01°
H1-C-O = 112.35°
C-N-O = 69.07°
C-N-H4 = 121.59°
C-N-H5 = 125.98°

Dihedral Angles
H1-C-N-H2 = 119.48°
H1-C-N-H3 = 128.44°
H1-C-N-O = –31.88°
H1-C-N-H4 = 68.21°
H1-C-N-H5 = –131.06°

Fig. 9 The CCSD(T)/aug-cc-pVTZ optimized transition state geometry of **TS1′**, connecting **M2** and **M5**. The bond lengths are shown in Angstroms with relevant bond angles and dihederal angles shown below.

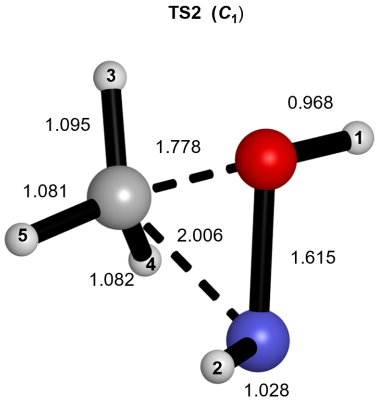

Bond Angles
H1-O-N = 99.74°
O-N-H2 = 96.06°
O-N-C = 57.60°
O-C-H3 = 89.42°
O-C-H4 = 118.92°
O-C-H5 = 109.36°

Dihedral Angles
H1-O-N-H2 = 142.59°
H1-O-N-C = –107.05°
O-N-C-H3 = 13.86°
O-N-C-H4 = 133.47°
O-N-C-H5 = –113.38°

Fig. 10 The CCSD(T)/aug-cc-pVTZ optimized transition state geometry of **TS2**, connecting **M3** and **M4**. The bond lengths are shown in Angstroms with relevant bond angles and dihederal angles shown below.

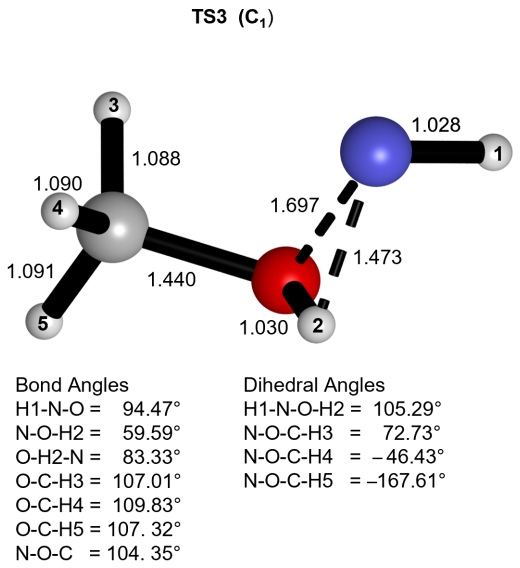

Fig. 11 The CCSD(T)/aug-cc-pVTZ optimized transition state geometry of **TS3**, connecting **M4** and **M5**. The bond lengths are shown in Angstroms with relevant bond angles and dihederal angles shown below.

knowledge, no search of the ISM has been conducted for **M2**. Structures **M3** and **M5** are further down the reaction pathways but also very likely to persist as they are in potential wells of at least 54.8 kcal mol^{-1}. The final minimum, **M4**, is not likely exist with any detectable abundance, because it has a barrier of only 2.7 kcal mol^{-1} to continue along the reaction pathway. Additionally, **M4** can only be formed after surpassing a substantial energetic barrier of 98.8 kcal mol^{-1}.

Conclusions

This research provides the most reliable characterization of the potential energy surface to date for the reaction between methylamine and O(^{1}D). We have optimized stationary points at the CCSD(T)/aug-cc-pVTZ level of theory and extrapolated energies to the CCSDT(Q)/CBS limit. All transition states were correctly connected to the proper minima and ensured to correspond to the appropriate chemical process via IRC and harmonic frequency computations. NBO computations were used to reinforce our chemical intuition for each reaction by means of Hammond's postulate. We found that five minimum structures exist on the potential energy surface, one of which (**M4**) was previously incorrectly assigned as a transition state. Our stationary points include a new transition state that links methylamine oxide to methoxyamine directly as well as a new transition state that connects N-methylhydroxylamine to CH_3OHNH. To the best of our knowledge, no spectroscopic study has been conducted to search for **M2** (methylamine oxide) or **M4** (CH_3OHNH) in the ISM. Our characterization of the potential energy surface predicts that **M1** (aminomethanol), **M2**, **M3** (n-methylhydroxylamine), and **M5** (methoxyamine) should be relatively abundant products of the reaction while **M4** is much less likely to be observed. Our research will be helpful in further prediction and detection of pre-biotic nitrogen containing species in the ISM.

Conflicts of interest

There are no conflicts to declare.

Acknowledgements

This work was supported by The Department of Energy, Office of Basic Energy Sciences (BES), Computational and Theoretical Chemistry (CTC) Program. Under Grant DE-SC0018412.

Notes and references

1 B. A. McGuire, P. B. Carroll, R. A. Loomis, I. A. Finneran, P. R. Jewell, A. J. Remijan and G. A. Blake, *Science*, 2016, **352**, 1449–1452.
2 D. Quan, E. Herbst, J. F. Corby, A. Durr and G. Hassel, *Astrophys. J.*, 2016, **824**, 129.
3 R. I. Kaiser, S. Maity and B. M. Jones, *Angew. Chem. Int. Edit.*, 2015, **54**, 195–200.
4 C. R. Arumainayagam, R. T. Garrod, M. C. Boyer, A. K. Hay, S. Tong Bao, J. S. Campbell, J. Wang, C. M. Nowak, M. R. Arumainayagam and P. J. Hodge, *Chemical Society Reviews*, 2019.
5 C. Meinert, I. Myrgorodska, P. Marcellus, T. Buhse, L. Nahon, S. V. Hoffmann, L. L. S. d'Hendecourt and U. J. Meierhenrich, *Science*, 2016, **352**, 208–212.
6 S. L. Miller, *Science, New Series*, 1953, **117**, 528–529.
7 J. R. Cronin and S. Pizzarello, *Adv. Space Res.*, 1983, **3**, 5–18.
8 J. Oró, *Nature*, 1961, **190**, 389.
9 J. R. Cronin and S. Chang, in *The Chemistry of Life's Origins*, ed. J. M. Greenberg, C. X. Mendoza-Gómez and V. Pirronello, Springer Netherlands, Dordrecht, 1993, pp. 209–258.
10 L. M. Ziurys, G. R. Adande, J. L. Edwards, D. R. Schmidt, D. T. Halfen and N. J. Woolf, *Orig Life Evol Biosph*, 2015, **45**, 275–288.
11 C. de Duve, *Orig Life Evol Biosph*, 2003, **33**, 559–574.
12 R. D. Brown, P. D. Godfrey, J. W. V. Storey, M.-P. Bassez, B. J. Robinson, R. A. Batchelor, M. G. McCulloch, O. E. H. Rydbeck and Ã. G. Hjalmarson, *Mon Not R Astron Soc*, 1979, **186**, 5P–8P.
13 J. M. Hollis, L. E. Snyder, R. D. Suenram and F. J. Lovas, *Astrophys. J.*, 1980, **241**, 1001–1006.
14 J. M. Hollis, J. A. Pedelty, D. A. Boboltz, S.-Y. Liu, L. E. Snyder, P. Palmer, F. J. Lovas and P. R. Jewell, *Astrophys. J.*, 2003, **596**, L235–L238.
15 L. E. Snyder, F. J. Lovas, J. M. Hollis, D. N. Friedel, P. R. Jewell, A. Remijan, V. V. Ilyushin, E. A. Alekseev and S. F. Dyubko, *Astrophys. J.*, 2005, **619**, 914–930.
16 M. R. Cunningham, P. A. Jones, P. D. Godfrey, D. M. Cragg, I. Bains, M. G. Burton, P. Calisse, N. H. M. Crighton, S. J. Curran, T. M. Davis, J. T. Dempsey, B. Fulton, M. G. Hidas, T. Hill, L. Kedziora-Chudczer, V. Minier, M. B. Pracy, C. Purcell, J. Shobbrook and T. Travouillon, *Mon Not R Astron Soc*, 2007, **376**, 1201–1210.
17 P. A. Jones, M. R. Cunningham, P. D. Godfrey and D. M. Cragg, *Mon Not R Astron Soc*, 2007, **374**, 579–589.
18 W. M. Irvine, *Orig Life Evol Biosph*, 1998, **28**, 365–383.

19 P. Ehrenfreund, M. P. Bernstein, J. P. Dworkin, S. A. Sandford and L. J. Allamandola, *Astrophys. J.*, 2001, **550**, L95–L99.

20 J. C. Aponte, J. E. Elsila, D. P. Glavin, S. N. Milam, S. B. Charnley and J. P. Dworkin, *ACS Earth and Space Chem.*, 2017, **1**, 3–13.

21 P. D. Holtom, C. J. Bennett, Y. Osamura, N. J. Mason and R. I. Kaiser, *Astrophys. J.*, 2005, **626**, 940–952.

22 A. Sato, Y. Kitazawa, T. Ochi, M. Shoji, Y. Komatsu, M. Kayanuma, Y. Aikawa, M. Umemura and Y. Shigeta, *Mol. Astrophys.*, 2018, **10**, 11–19.

23 M. P. Bernstein, J. P. Dworkin, S. A. Sandford, G. W. Cooper and L. J. Allamandola, *Nature*, 2002, **416**, 401–403.

24 G. M. Muñoz Caro, U. J. Meierhenrich, W. A. Schutte, B. Barbier, A. Arcones Segovia, H. Rosenbauer, W. H.-P. Thiemann, A. Brack and J. M. Greenberg, *Nature*, 2002, **416**, 403–406.

25 D. T. Halfen, V. V. Ilyushin and L. M. Ziurys, *Astrophys. J.*, 2013, **767**, 66.

26 L. Kolesniková, E. R. Alonso, S. Mata and J. L. Alonso, *J. Mol. Spectrosc.*, 2017, **335**, 54–60.

27 L. Kolesniková, B. Tercero, E. R. Alonso, J.-C. Guillemin, J. Cernicharo and J. L. Alonso, *Astron. Astrophys.*, 2018, **609**, A24.

28 J. Woodall, M. Agúndez, A. J. Markwick-Kemper and T. J. Millar, *Astron. Astrophys.*, 2007, **466**, 1197–1204.

29 R. T. Garrod and E. Herbst, *Astron. Astrophys.*, 2006, **457**, 927–936.

30 A. Schriver, L. Schriver-Mazzuoli, P. Ehrenfreund and L. ́d Hendecourt, *Chem. Phys.*, 2007, **334**, 128–137.

31 A. Horn, H. Møllendal, O. Sekiguchi, E. Uggerud, H. Roberts, E. Herbst, A. Viggiano and T. Fridgen, *Astrophys. J.*, 2004, **611**, 605–614.

32 A. G. G. M. Tielens and W. Hagen, *Astron. Astrophys.*, 1982, **114**, 245–260.

33 P. Theule, F. Borget, F. Mispelaer, G. Danger, F. Duvernay, J. C. Guillemin and T. Chiavassa, *Astron. Astrophys.*, 2011, **534**, A64.

34 R. T. Garrod, *Astrophys. J.*, 2013, **765**, 60.

35 R. T. Garrod, S. L. W. Weaver and E. Herbst, *Astrophys. J.*, 2008, **682**, 283–302.

36 A. G. G. M. Tielens, *Rev. Mod. Phys.*, 2013, **85**, 1021–1081.

37 B. M. Hays and S. L. Widicus Weaver, *J. Phys. Chem. A*, 2013, **117**, 7142–7148.

38 N. Kaifu, M. Morimoto, K. Nagane, K. Akabane, T. Iguchi and K. Takagi, *Astrophys. J.*, 1974, **191**, L135–L137.

39 N. Fourikis, K. Takagi and M. Morimoto, *Astrophys. J.*, 1974, **191**, L139.

40 N. Kaifu, K. Takagi and T. Kojima, *Astrophys. J. Lett.*, 1975, **198**, L85–L88.

41 J. Cernicharo, Z. Kisiel, B. Tercero, L. Kolesniková, I. R. Medvedev, A. López, S. Fortman, M. Winnewisser, F. C. d. Lucia, J. L. Alonso and J.-C. Guillemin, *A&A*, 2016, **587**, L4.

42 L. Kolesniková, E. R. Alonso, B. Tercero, J. Cernicharo and J. L. Alonso, *A&A*, 2018, **616**, A173.

43 R. L. Pulliam, B. A. McGuire and A. J. Remijan, *Astrophys. J.*, 2012, **751**, 1.

44 V. A. Basiuk, *J. Phys. Chem. A*, 2001, **105**, 4252–4258.

45 A. Largo, P. Redondo and C. Barrientos, *Int. J. Quantum Chem.*, 2004, **98**, 355–360.

46 P. Redondo, A. Largo and C. Barrientos, *Astron. Astrophys.*, 2015, **579**, A125.

47 R. Spezia, Y. Jeanvoine and D. Scuderi, in *Origin and Evolution of Biodiversity*, ed. P. Pontarotti, Springer International Publishing, Cham, 2018, pp. 277–292.

48 O. Roncero, A. Zanchet and A. Aguado, *Phys. Chem. Chem. Phys.*, 2018, **20**, 25951–25958.

49 L. MargulÃĺs, B. A. McGuire, M. L. Senent, R. A. Motiyenko, A. Remijan and J. C. Guillemin, *A&A*, 2017, **601**, A50.

50 F. Lique, I. JimÃľnez-Serra, S. Viti and S. Marinakis, *Phys. Chem. Chem. Phys.*, 2018, **20**, 5407–5414.

51 P. Redondo, H. MartÃ■nez, A. Largo and C. Barrientos, *A&A*, 2017, **603**, A139.

52 J. C. Loison and K. M. Hickson, *Chem. Phys. Lett.*, 2015, **635**, 174–179.

53 J. B. Bergner, K. I. Öberg and M. Rajappan, *Astrophys. J.*, 2017, **845**, 29.

54 H. Yamazaki and R. J. Cvetanović, *J. Chem. Phys.*, 1964, **41**, 3703–3710.

55 C.-K. Huang, Z.-F. Xu, M. Nakajima, H. M. T. Nguyen, M. C. Lin, S. Tsuchiya and Y.-P. Lee, *J. Chem. Phys.*, 2012, **137**, 164307.

56 C. Lugez, A. Schriver, R. Levant and L. Schriver-Mazzuoli, *Chem. Phys.*, 1994, **181**, 129–146.

57 N. Balucani, F. Leonori, R. Petrucci, M. Stazi, D. Skouteris, M. Rosi and P. Casavecchia, *Faraday Discuss.*, 2010, **147**, 189–216.

58 N. Balucani, D. Skouteris, F. Leonori, R. Petrucci, M. Hamberg, W. D. Geppert, P. Casavecchia and M. Rosi, *J. Phys. Chem. A*, 2012, **116**, 10467–10479.

59 F. Leonori, D. Skouteris, R. Petrucci, P. Casavecchia, M. Rosi and N. Balucani, *J. Chem. Phys.*, 2013, **138**, 024311.

60 A. Melli, M. Melosso, N. Tasinato, G. Bosi, L. Spada, J. Bloino, M. Mendolicchio, L. Dore, V. Barone and C. Puzzarini, *Astrophys. J.*, 2018, **855**, 123.

61 M. T. Feldmann, S. L. Widicus, G. A. Blake, D. R. Kent and W. A. Goddard, *J. Chem. Phys.*, 2005, **123**, 034304.

62 F. Neese, *Wires. Comput. Mol. Sci.*, 2012, **2**, 73–78.

63 A. D. Becke, *J. Chem. Phys.*, 1993, **98**, 5648–5652.

64 F. Weigend and R. Ahlrichs, *Phys. Chem. Chem. Phys.*, 2005, **7**, 3297–3305.

65 I. Shavitt and R. J. Bartlett, *Many-Body Methods in Chemistry and Physics: MBPT and Coupled-Cluster Theory*, Cambridge University Press, 2009.

66 R. J. Bartlett, J. D. Watts, S. A. Kucharski and J. Noga, *Chem. Phys. Letters*, 1990, **165**, 513–522.

67 J. F. Stanton, *Chem. Phys. Letters*, 1997, **281**, 130–134.

68 K. Raghavachari, G. W. Trucks, J. A. Pople and M. Head-Gordon, *Chem. Phys. Letters*, 1989, **157**, 479–483.

69 J. F. Stanton, J. Gauss, L. Cheng, M. E. Harding, D. A. Matthews and P. G. Szalay, *CFOUR, Coupled-Cluster techniques for Computational Chemistry, a quantum-chemical program package*, With contributions from A.A. Auer, R.J. Bartlett, U. Benedikt, C. Berger, D.E. Bernholdt, Y.J. Bomble, O. Christiansen, F. Engel, R. Faber, M. Heckert, O. Heun, M. Hilgenberg, C. Huber, T.-C. Jagau, D. Jonsson, J. Jusélius, T. Kirsch, K. Klein, W.J. Lauderdale, F. Lipparini, T. Metzroth, L.A. Mück, D.P. O'Neill, D.R. Price, E. Prochnow, C. Puzzarini, K. Ruud, F. Schiffmann, W. Schwalbach, C. Simmons, S. Stopkowicz, A. Tajti, J. Vázquez, F. Wang, J.D. Watts and the integral packages MOLECULE (J. Almlöf and P.R. Taylor), PROPS (P.R. Taylor), ABACUS (T. Helgaker, H.J. Aa. Jensen, P. Jørgensen, and J. Olsen), and ECP routines by A. V. Mitin and C. van Wüllen. For the current version, see http://www.cfour.de.

70 T. H. Dunning, *J. Chem. Phys.*, 1989, **90**, 1007–1023.

71 R. M. Parrish, L. A. Burns, D. G. A. Smith, A. C. Simmonett, A. E. DePrince, E. G. Hohenstein, U. Bozkaya, A. Y. Sokolov, R. Di Remigio, R. M. Richard, J. F. Gonthier, A. M. James, H. R. McAlexander, A. Kumar, M. Saitow, X. Wang, B. P. Pritchard, P. Verma, H. F. Schaefer, K. Patkowski, R. A. King, E. F. Valeev, F. A. Evangelista, J. M. Turney, T. D. Crawford and C. D. Sherrill, *J. Chem. Theory Comput.*, 2017, **13**, 3185–3197.

72 M. S. Schuurman, S. R. Muir, W. D. Allen and H. F. Schaefer, *J. Chem. Phys.*, 2004, **120**, 11586–11599.

73 J. M. Gonzales, C. Pak, R. S. Cox, W. D. Allen, H. F. Schaefer, A. G. Csaszar and G. Tarczay, *Chem. Eur. J.*, 2003, **9**, 2173–2192.

74 A. G. Császár, W. D. Allen and H. F. Schaefer, *J. Chem. Phys.*, 1998, **108**, 9751–9764.

75 A. L. L. East and W. D. Allen, *J. Chem. Phys.*, 1993, **99**, 4638–4650.

76 C. E. Moore, *Tables of Spectra of Hydrogen, Carbon, Nitrogen, and Oxygen Atoms and Ions*, 1993.

77 D. Feller, K. A. Peterson and T. D. Crawford, *J. Chem. Phys.*, 2006, **124**, 054107.

78 T. Helgaker, W. Klopper, H. Koch and J. Noga, *J. Chem. Phys.*, 1997, **106**, 9639–9646.

79 J. Noga and R. J. Bartlett, *J. Chem. Phys.*, 1987, **86**, 7041–7050.

80 G. E. Scuseria and H. F. Schaefer, *Chem. Phys. Letters*, 1988, **152**, 382–386.

81 E. Papajak and D. G. Truhlar, *J. Chem. Theory Comput.*, 2011, **7**, 10–18.

82 Y. J. Bomble, J. F. Stanton, M. Kállay and J. Gauss, *J. Chem. Phys.*, 2005, **123**, 054101.

83 M. Kállay and J. Gauss, *J. Chem. Phys.*, 2008, **129**, 144101.

84 S. Stopkowicz and J. Gauss, *J. Chem. Phys.*, 2008, **129**, 164119.

85 H. Sellers and P. Pulay, *Chem. Phys. Letters*, 1984, **103**, 463–465.

86 N. C. Handy and H. F. Yamaguchi, Yukio and, *Journal of Chem. Phys.*, 1986, **84**, 4481.

87 E. D. Glendening, C. R. Landis and F. Weinhold, *Wires. Comput. Mol. Sci.*, 2012, **2**, 1–42.

88 E. D. Glendening, C. R. Landis and F. Weinhold, *J. Comput. Chem.*, 2013, **34**, 1429–1437.

89 S. A. Kucharski and R. J. Bartlett, *Theoret. Chim. Acta*, 1991, **80**, 387–405.

90 N. Oliphant and L. Adamowicz, *J. Chem. Phys.*, 1991, **95**, 6645–6651.

91 S. A. Kucharski and R. J. Bartlett, *J. Chem. Phys.*, 1992, **97**, 4282–4288.

92 G. S. Hammond, *J. Am. Chem. Soc.*, 1955, **77**, 334–338.